A divalent cation-dependent variant of the *glmS* ribozyme with stringent Ca^{2+} selectivity co-opts a preexisting nonspecific metal ion-binding site

MATTHEW W.L. LAU, ROBERT J. TRACHMAN III, and ADRIAN R. FERRÉ-D'AMARÉ
National Heart, Lung and Blood Institute, Bethesda, Maryland 20892-8012, USA

ABSTRACT

Ribozymes use divalent cations for structural stabilization, as catalytic cofactors, or both. Because of the prominent role of Ca^{2+} in intracellular signaling, engineered ribozymes with stringent Ca^{2+} selectivity would be important in biotechnology. The wild-type *glmS* ribozyme (*glmS*^{WT}) requires glucosamine-6-phosphate (GlcN6P) as a catalytic cofactor. Previously, a *glmS* ribozyme variant with three adenosine mutations (*glmS*^{AAA}) was identified, which dispenses with GlcN6P and instead uses, with little selectivity, divalent cations as cofactors for site-specific RNA cleavage. We now report a Ca^{2+}-specific ribozyme (*glmS*^{Ca}) evolved from *glmS*^{AAA} that is >10,000 times more active in Ca^{2+} than Mg^{2+}, is inactive in even 100 mM Mg^{2+}, and is not responsive to GlcN6P. This stringent selectivity, reminiscent of the protein nuclease from *Staphylococcus*, allows rapid and selective ribozyme inactivation using a Ca^{2+} chelator such as EGTA. Because *glmS*^{Ca} functions in physiologically relevant Ca^{2+} concentrations, it can form the basis for intracellular sensors that couple Ca^{2+} levels to RNA cleavage. Biochemical analysis of *glmS*^{Ca} reveals that it has co-opted for selective Ca^{2+} binding a nonspecific cation-binding site responsible for structural stabilization in *glmS*^{WT} and *glmS*^{AAA}. Fine-tuning of the selectivity of the cation site allows repurposing of this preexisting molecular feature.

Keywords: catalytic RNA; in vitro selection; phosphorothioate interference; SAXS; molecular exaptation

INTRODUCTION

Divalent cations stabilize the 3D architecture of ribozymes and other structured RNAs (for review, see Draper 2004; Koculi et al. 2007). In addition, alkaline earth ions directly participate in the catalytic mechanism of several ribozymes (for review, see Fedor and Williamson 2005; Ferré-D'Amaré and Scott 2010; Aufinger et al. 2011). The specific identity of the divalent cation is generally less important for electrostatic structural stabilization than for catalytic cofactor function. For instance, the *Tetrahymena* ribozyme can adopt a near-native fold in the presence of Ca^{2+}, Ba^{2+}, or Sr^{2+}, but is inactive unless its active site is bound to Mg^{2+} (Grosshans and Cech 1989; Celander and Cech 1991; Koculi et al. 2007). Structure-guided engineering and in vitro evolution have been used to alter the cation specificity of several natural ribozymes. In the case of the *Tetrahymena* ribozyme, in vitro selection produced variants that have 300-fold increased activity in Ca^{2+} (Lehman and Joyce 1993; Riley and Lehman 2003). However, these also had increased activity in Mg^{2+}. Biochemical analyses suggested that their active sites did not acquire specificity for Ca^{2+}; instead they relaxed their cation selectivity (Cernak et al. 2008). Similarly, in vitro evolution of the ribonuclease P ribozyme for cleavage in Ca^{2+} produced a point mutant that acquired the ability to cleave in this cation. However, and despite a decrease of reactivity in Mg^{2+}, the cleavage rate of the mutant in Ca^{2+} was only 91-fold higher than in Mg^{2+} (Frank and Pace 1997). Consistent with its intracellular abundance, Mg^{2+} is preferentially used by most natural ribozymes that depend on a divalent cation as a catalytic cofactor. Ribozymes specific for Ca^{2+} would have biotechnological applications, given the importance of this metal ion in intracellular signaling (for review, see Clapham 2007). Altering the cation selectivity of natural ribozymes so that they are stringently dependent on Ca^{2+} has remained a challenging molecular engineering problem.

The *glmS* ribozyme is a bacterial gene-regulatory RNA that controls the abundance of glucosamine-6-phosphate (GlcN6P), an essential precursor for cell-wall biosynthesis (for review, see Ferré-D'Amaré 2010). It is part of the mRNA for the enzyme GlcN6P synthetase. GlcN6P binds to the ribozyme and activates its self-cleavage (Winkler et al.

Corresponding author: adrian.ferre@nih.gov
Article is online at http://www.rnajournal.org/cgi/doi/10.1261/rna.059824.116.

2004). This leads to degradation of the mRNA, thereby enabling negative-feedback regulation of GlcN6P synthesis (Collins et al. 2007). Uniquely among self-cleaving RNAs, the *glmS* ribozyme uses an exogenous small molecule, GlcN6P, as an obligate catalytic cofactor (Klein and Ferré-D'Amaré 2006; Viladoms and Fedor 2012). Consistent with the coenzyme function of GlcN6P, the activity of this ribozyme is largely insensitive to the identity of divalent cations. Thus, and as expected for their role solely in structural stabilization, the *glmS* ribozyme exhibits comparable GlcN6P-catalyzed activity in the presence of Mg^{2+}, Ca^{2+}, Mn^{2+}, or even the complex ion cobalt (III) hexammine (Roth et al. 2006; Klawuhn et al. 2010). The amino ligands of the latter are kinetically inert, and therefore activity of the ribozyme in this compound is strong evidence that inner-sphere cation coordination is not required for folding or catalysis (Cowan 1993).

Previously, we examined whether RNAs closely related to the wild-type *glmS* ribozyme (*glmS*^{WT}) could perform divalent cation-mediated catalysis without using the coenzyme GlcN6P (Lau and Ferré-D'Amaré 2013). The evolutionary ancestors of *glmS*^{WT} could have been such unregulated ribozymes. Acquisition of GlcN6P-dependence by RNAs like these would have given rise to the gene-regulatory capability of the present-day *glmS*^{WT} (Ferré-D'Amaré 2011). We discovered that three adenosine mutations in the ribozyme core produced a variant (termed *glmS*^{AAA}) that is fully active ($k_{obs} \sim 2.5\ min^{-1}$, which is within 20-fold of *glmS*^{WT}) in the presence of divalent cations alone. This mutant ribozyme was not stimulated by GlcN6P. As is the case for many engineered variants of natural ribozymes, *glmS*^{AAA} has only modest cation specificity; its maximum activity in Ca^{2+} exceeds that in Mg^{2+} by less than a factor of 50 (Lau and Ferré-D'Amaré 2013).

The crystal structure of *glmS*^{AAA} revealed essentially the same 3D-architecture as that of *glmS*^{WT}, underscoring the high stability of this ribozyme fold, and demonstrating that this RNA structural scaffold can be functionalized to support divergent biochemical activities (GlcN6P and cation-mediated catalysis by *glmS*^{WT} and *glmS*^{AAA}, respectively; Lau and Ferré-D'Amaré 2013). The functional plasticity of the structurally rigid *glmS* ribozyme fold we uncovered suggested that other variants that exhibit a higher degree of cation selectivity than *glmS*^{AAA} might exist. To test this hypothesis, we performed further in vitro selection experiments to isolate variants of the *glmS* ribozyme that are selectively activated by Ca^{2+}. Such RNAs could potentially be developed into tools that link intracellular signaling by Ca^{2+} with RNA stability and gene expression. Unlike in the *glmS*^{AAA} selection (Lau and Ferré-D'Amaré 2016a), these new experiments explicitly selected and counterselected for catalysis based on the identity of the divalent cation (Ca^{2+} versus Mg^{2+}) in solution. This work has now produced a mutant of the *glmS* ribozyme that does not use GlcN6P for catalysis and is exquisitely selective for Ca^{2+}. Small-angle X-ray scattering (SAXS) demonstrates that the mutant can fold equally in Ca^{2+} or Mg^{2+}, excluding a primarily structural role for the cation. Biochemical analysis indicates that rather than evolving a new Ca^{2+}-binding site, the mutant RNA co-opted a nonspecific cation-binding site that had played a structural role in both the *glmS*^{WT} and *glmS*^{AAA} ribozymes.

RESULTS

In vitro selection yields a highly Ca^{2+}-selective *glmS* ribozyme variant

To seek variants of the *glmS* ribozyme that function without GlcN6P and are highly selective for specific metal ions, we performed in vitro selection using a pool of RNA sequences based on *glmS*^{AAA} in which nucleotides near the active site that do not participate in forming the characteristic, triply pseudoknotted secondary structure (Klein and Ferré-D'Amaré 2006) of the ribozyme were mutagenized (Fig. 1), and enriched for cleavage in either Mg^{2+} or Ca^{2+} (Materials and Methods). Ribozymes with varying degrees of selectivity for Ca^{2+} were isolated after eight selection rounds (Fig. 2).

A group of ribozymes that displayed strong discrimination against Mg^{2+} was chosen for further analyses. These RNAs all have in common 10 point mutations from the wild-type sequence (eight mutations relative to *glmS*^{AAA}; Figs. 1B, 3), and reversion of any of these to the wild-type nucleotide reduced or eliminated Ca^{2+}-dependent activity (not shown). A ribozyme containing just these mutations (hereafter *glmS*^{Ca}) displayed high selectivity for Ca^{2+}. Its cleavage rate was at least 10,000-fold faster in 2 mM Ca^{2+} than in 2 mM Mg^{2+}. This is a lower bound because this ribozyme exhibited no detectable activity in Mg^{2+}, and therefore the estimate is limited by the sensitivity of our cleavage assay. Even in the presence of 100 mM Mg^{2+} (Fig. 4A), *glmS*^{Ca} was inactive. This Ca^{2+}-selective ribozyme is also inactive in common monovalent and lanthanide ions and the soft divalent ion Cd^{2+}, but exhibits residual activity in Sr^{2+} (Fig. 4A). Like *glmS*^{AAA} (Lau and Ferré-D'Amaré 2013), *glmS*^{Ca} is inactive in cobalt hexammine, indicating that it requires inner-sphere cation coordination for activity.

Comparison of the activity of *glmS*^{Ca} in the presence and absence of GlcN6P shows no stimulation by the cofactor of *glmS*^{WT} (Table 1). Indeed, *glmS*^{Ca} is not stimulated by a number of other small molecule activators of *glmS*^{WT} with vicinal amine and hydroxyl groups (McCarthy et al. 2005; Lim et al. 2006; Posakony and Ferré-D'Amaré 2013; Fei et al. 2014), nor a recently synthesized GlcN6P analog activator of *glmS*^{WT} that bears a guanidinium group instead of the amine (Table 1). Thus, *glmS*^{Ca}, like *glmS*^{AAA} from which it evolved, is a small molecule cofactor-independent ribozyme.

Mg^{2+} inhibits *glmS*^{Ca} catalysis but not folding

Kinetic analysis shows that *glmS*^{Ca} attains half-maximal activity ($K_{1/2}$) at 14 mM Ca^{2+} (in the presence of 100 mM KCl) (Fig.

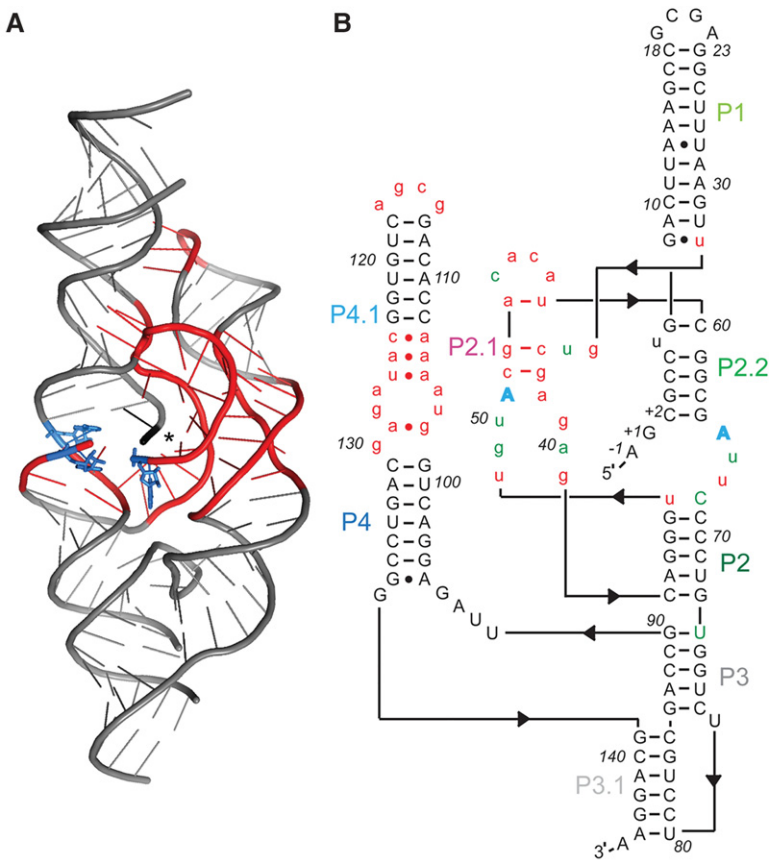

FIGURE 1. Mutagenized RNA pool based on $glmS^{AAA}$ for in vitro selection. (*A*) Cartoon depiction of the crystal structure of $glmS^{AAA}$ (Lau and Ferré-D'Amaré 2013). Nucleotides mutagenized for this study are in red. Blue residues denote the three adenosine mutations (relative to wild-type, A49, A51, G65) that characterize $glmS^{AAA}$. (*) Location of scissile phosphate. (*B*) Sequence and hypothetical secondary structure of $glmS^{Ca}$. Nucleotides in red lower case were mutagenized by 30% relative to $glmS^{AAA}$. Nucleotides in gray were constant. Two of the three adenosine mutations that characterize $glmS^{AAA}$ (blue) were retained in $glmS^{Ca}$. Nucleotides in green denote the eight mutations in $glmS^{Ca}$ relative to $glmS^{AAA}$.

To examine whether $glmS^{Ca}$ requires Ca^{2+} for folding, we compared its overall three-dimensional structure in solution in the presence of a near-physiological concentration of $MgCl_2$ (Romani and Scarpa 1992; Grubbs 2002), or the same concentration of $CaCl_2$ or $SrCl_2$ (2.5 mM of the alkaline earth salt in addition to 100 mM KCl in each case, Materials and Methods) by small-angle X-ray scattering (SAXS). In the presence of Mg^{2+}, $glmS^{Ca}$ exhibits a radius of gyration (R_g) of 41.4 ± 1.2 Å. Unexpectedly, given the inactivity of the ribozyme in Mg^{2+}, the shapes of its pair-probability distribution function $P(r)$ (Fig. 5A) and Kratky plots (Fig. 5B) are indicative of a folded RNA. The R_g of the RNA in the presence of either Ca^{2+} or Sr^{2+} is identical within experimental error to that in Mg^{2+}. Moreover, the $P(r)$ and Kratky plots of the RNA in the three divalent cations tested are virtually identical (Fig. 5B). This analysis indicates that all three divalent cations can globally fold the RNA to a comparable extent at the same ionic strength. SAXS analysis, therefore, suggests that inactivity of $glmS^{Ca}$ in Mg^{2+} reflects inhibition of the chemical step, rather than a deficit in folding. Under our experimental conditions, the R_g of the $glmS^{AAA}$ ribozyme (in the equivalent *cis*-acting form) in 2.5 mM $MgCl_2$ is 38.5 ± 2.3 Å (not shown), suggesting that the parental ribozyme may be slightly more compact than $glmS^{Ca}$.

4B). This is lower than for $glmS^{WT}$ (in saturating GlcN6P and 100 mM KCl) and $glmS^{AAA}$ ($K_{1/2}$ = 31 and 93 mM, respectively, Lau and Ferré-D'Amaré 2013), indicating a higher affinity for the divalent cation. Addition of 5 mM Mg^{2+} to the Ca^{2+} titration of $glmS^{Ca}$ yielded a sigmoidal relationship, and increased $K_{1/2}$ by approximately twofold (Fig. 4B). Lineweaver–Burk analysis shows a nonlinear relationship in the presence of Mg^{2+}, suggestive of mixed-type inhibition by this cation (Fig. 4C). Competition by Mg^{2+} with Ca^{2+} for inner-sphere binding to functionally important sites is further supported by analogous experiments in which a Ca^{2+} titration was supplemented with 5 mM Ba^{2+}. In these, the $K_{1/2}$ was increased by ~1.5 fold, but the kinetics remained Michaelis–Menten. Presumably, the larger ionic radius of Ba^{2+} (Table 2) precludes it from competing efficiently for functionally important inner-sphere Ca^{2+} binding sites, but it can displace some diffusely RNA-associated (Draper 2004) Ca^{2+} ions (Fig. 4B).

The $glmS^{Ca}$ ribozyme cleaves one nucleotide 3′ to $glmS^{WT}$

Both $glmS^{WT}$ and $glmS^{AAA}$ cleave RNA by internal transesterification, yielding products with 2′,3′-cyclic phosphate and 5′-OH termini (Winkler et al. 2004; Lau and Ferré-D'Amaré 2013). To characterize the cleavage reaction of

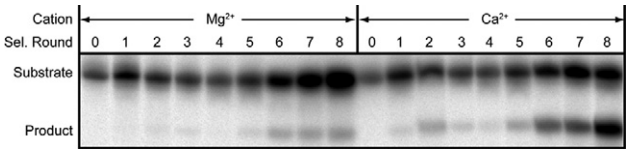

FIGURE 2. In vitro selection of cation-specific ribozymes from $glmS^{AAA}$. RNAs from each of eight rounds in the Ca^{2+}-specific selection (Pool B, Materials and Methods) were ^{32}P-body-labeled and incubated in either 25 mM Mg^{2+} or 25 mM Ca^{2+} for 1 h. Samples were analyzed by denaturing PAGE and visualized by autoradiography.

FIGURE 3. Alignment of sequences from three selections after nine rounds. (*A*) Mg^{2+}-dependent selection, pool A. (*B*) Ca^{2+}-dependent selection, pool B. (*C*) Ca^{2+}-dependent selection with mutagenic PCR, pool C (Materials and Methods). Nucleotides in red were mutagenized by 30% relative to *glmS*^{AAA} in the selection pool. Nucleotides in black were constant. The three adenosines that characterize *glmS*^{AAA} are in cyan. The eight mutations in *glmS*^{Ca} (relative to *glmS*^{AAA}) are boxed in green. For comparison, *glmS*^{WT} and *glmS*^{AAA} sequences are shown at the *bottom* of each panel. Paired (duplex) regions of *glmS*^{WT} and *glmS*^{AAA} are labeled as in Figure 1A.

glmS^{Ca}, we compared its 5′ cleavage product with those of *glmS*^{WT} and *glmS*^{AAA}. Upon treatment of the 5′ cleavage products of the three ribozymes with acid or polynucleotide kinase, they exhibited parallel gel mobility shifts consistent with opening and removal, respectively, of a 2′,3′-cyclic phosphate (Fig. 6A). This suggests that *glmS*^{Ca}-catalyzed RNA cleavage also proceeds through internal transesterification.

Unexpectedly, the 5′ cleavage product of *glmS*^{Ca} had an electrophoretic mobility consistent with being one nucleotide longer than the products of the two other RNAs. This hinted that the cleavage site of the Ca^{2+}-selective ribozyme shifted one nucleotide 3′ to the cleavage site of the wild type. To confirm this, we subjected oligonucleotides bearing a 2′-deoxyribose at positions −2, −1, or +1 (by convention, there is no zero position) to cleavage by the three ribozymes (Fig. 6B). Because the 2′-OH group is the nucleophile in the transesterification reaction, substitution of the reactive ribose with a deoxyribose is expected to abrogate cleavage. Consistent with previous experiments, *glmS*^{WT} and *glmS*^{AAA} cleavage was dependent on a 2′-OH at position −1 (Winkler et al. 2004; Lau and Ferré-D'Amaré 2013). In contrast, *glmS*^{Ca} could cleave a substrate with the deoxy substitution at position −1, but not at position +1. Overall, these experiments indicate that *glmS*^{Ca} cleaves its substrate between positions +1 and +2 by using the ribose 2′-OH of the former as the nucleophile.

Phosphorothioate interference suggests location of an essential Ca^{2+}

To locate Ca^{2+} ions important for *glmS*^{Ca} activity, we performed phosphorothioate interference mapping. This technique exploits the altered affinity for hard cations (e.g., Mg^{2+} or Ca^{2+}) resulting from substitution of nonbridging phosphate oxygen (NBPO) atoms of an RNA with sulfur (Schatz et al. 1991). We synthesized *glmS*^{Ca} analogs with random sulfur substitution of *pro*-R_P NBPOs by transcription, and separated active from inactive RNAs by electrophoresis following self-cleavage. Positions within *glmS*^{Ca} with deleterious substitutions were identified by comparing the relative abundance of active versus inactive RNA fragments after selective phosphorothioate cleavage with iodine. In our mapping analysis of *glmS*^{Ca}, which provided readout between residues G3 and G90, we observed strong interferences only at residues A40 and G41 (Fig. 7).

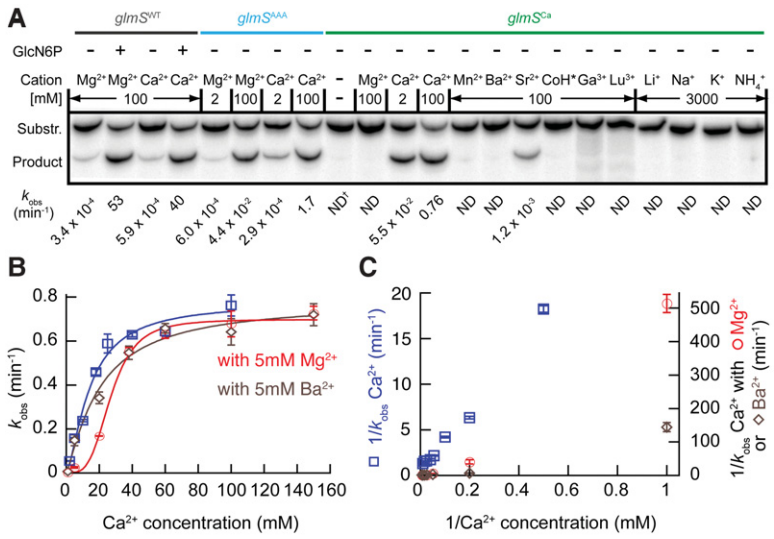

FIGURE 4. The *glmS*^{Ca} ribozyme is highly Ca^{2+}-selective. (*A*) *glmS*^{Ca} activity in the presence of various metal ions. Autoradiogram of PAGE analysis of cleavage of a 5′ ^{32}P-radiolabeled decanucleotide by different ribozymes for 30 min. Reaction rates are indicated. (*) Cobalt hexammine (CoH); (†) not determined (ND). (*B*) *glmS*^{Ca} activity in different Ca^{2+} concentrations (blue) and in the presence of an additional 5 mM Mg^{2+} (red) or 5 mM Ba^{2+} (brown). All reactions were in the presence of a background of 100 mM KCl. (*C*) Lineweaver–Burk representation of the reaction rates from *B*. Error bars represent standard errors of the mean of at least three independent experiments.

Previously, we identified functionally important divalent cations for *glmS*^{WT} and *glmS*^{AAA} by combining unbiased interference mapping and site-specific phosphorothioate substitution. We found that for both RNAs, the *pro*-R_P NBPO of residue C2 is important in metal ion coordination. The best ordered structural metal ion discovered in multiple crystallographic analyses of the two ribozymes (Fig. 8A) is coordinated by this oxygen atom (Klein and Ferré-D'Amaré 2006; Cochrane et al. 2007, 2009; Klein et al. 2007a,b). This hexacoordinate cation, M_A, is too far from the cleavage sites of either *glmS*^{WT} or *glmS*^{AAA} to participate directly in catalysis. Moreover, full activity of *glmS*^{WT} in cobalt hexammine (Roth et al. 2006) strongly argues against any essential direct (i.e., inner-sphere) role for this, or any other divalent cation in folding or catalysis by the wild-type ribozyme (Cowan 1993).

Activity of *glmS*^{AAA} was also dependent on metal ion coordination by the *pro*-R_P NBPO of residue A38 and the *pro*-S_P NBPO of residue C2 (Lau and Ferré-D'Amaré 2013). Crystallographic analysis confirmed the presence of a divalent cation bound at this position (M_B). Multiple lines of evidence indicated that this cation participates directly in the catalytic mechanism of *glmS*^{AAA} (but not *glmS*^{WT}). In contrast, we did not observe any significant interference at A38 for *glmS*^{Ca}, which implies that this ribozyme does not require M_B for catalysis. The interference at residues A40 and G41 of *glmS*^{Ca} is consistent with the presence of a metal ion (M_C) observed in crystal structures of *glmS*^{WT} and *glmS*^{AAA} (Fig. 8B). M_C is too far from the active site of *glmS*^{Ca} to participate in catalysis, and thus probably plays a structural role in all three ribozymes.

If neither M_B nor M_C is involved in catalysis by *glmS*^{Ca}, where is the essential metal ion cofactor? Examination of crystal structures suggests that by virtue of its novel cleavage site one nucleotide 3′ to the scissile phosphates of *glmS*^{WT} and *glmS*^{AAA}, *glmS*^{Ca} may recruit M_A for catalysis (Fig. 8B). We tested this by site-specific phosphorothioate substitution. Consistent with lack of involvement of M_B in catalysis by *glmS*^{Ca}, sulfur substitution of the *pro*-S_P NBPO of C2 only reduced the maximal cleavage fraction to ~80% (Fig. 8C). In contrast, substitution of the *pro*-R_P NBPO of C2, which coordinates M_A, markedly impaired *glmS*^{Ca} activity, with the maximum extent of cleavage reduced to ~9%. This impairment could not be relieved with Sr^{2+}, which suggests a high degree of cation selectivity of the M_A site in *glmS*^{Ca} (it could also not be rescued with the thiophilic cation Cd^{2+}, in which the ribozyme is inactive, not shown). Substitution of both NBPOs at G3 had no effect on activity, arguing against a nonlocal, nonspecific effect of sulfur substitution. Finally, we confirmed the importance of the structural cation M_C suggested by our mapping results by synthesizing *glmS*^{Ca} constructs containing a diastereomeric mixture of phosphorothioates at residues A40 and G41 (the internal position of the substitution precluded

TABLE 1. Reaction rates of *glmS*^{WT} and *glmS*^{Ca} with different GlcN6P analogs, at 5 mM concentration, in either 25 mM Mg^{2+} or 18 mM Ca^{2+}

Small molecule	*glmS*^{WT} in Mg^{2+} (min^{-1})	*glmS*^{Ca} in Mg^{2+} (min^{-1})	*glmS*^{Ca} in Ca^{2+} (min^{-1})
Glucosamine 6-phosphate	34 ± 1.9[a]	Not detectable	0.46 ± 0.01
3-azido-glucosamine	0.08 ± 0.003	Not detectable	0.36 ± 0.05
6-azidoglucosamine	0.4 ± 0.05	Not detectable	0.37 ± 0.01
2, 6-diaminoglucose	0.5 ± 0.02	Not detectable	0.32 ± 0.04
2-deoxy-2-guanidinylglucose-6-phosphate	0.6 ± 0.02	Not detectable	0.30 ± 0.02

[a]Rate reported previously (Lau and Ferré-D'Amaré 2013).

TABLE 2. Properties of select divalent cations

Cation	Ionic radius (pm)[a]	Absolute hardness (η)[b]	Coordination numbers
Mg^{2+}	86	32.55	4, 5, 6, 8
Cd^{2+}	109	10.29	4, 5, 6, 7, 8, 12
Ca^{2+}	114	19.52	6, 7, 8, 9, 10
Sr^{2+}	132	16.3	6, 7, 8, 9, 10, 12
Ba^{2+}	149	12.8	6, 7, 8, 9, 10, 11, 12

[a]Radii are for the hexacoordinate cations (Huheey 1983).
[b]Absolute hardness values from Parr and Pearson (1983) and Pearson (1988).

chromatographic resolution of the diastereomers). These had moderately impaired activity that could be partially relieved by Sr^{2+} (Fig. 8C). Overall, our analysis indicates that M_A is essential for *glmS*^{Ca} activity, without precluding a role in facilitating overall ribozyme folding.

DISCUSSION

Ten point mutations distinguish *glmS*^{Ca} from the GlcN6P-dependent wild-type ribozyme (Figs. 1, 3). Two of these, U49A and G65A, are shared with *glmS*^{AAA}. Previous analyses of *glmS*^{AAA} demonstrated that while both adenosine mutations contribute to the coenzyme-independence of that ribozyme, the mutation at position 65 is the most important in abrogating the ability of the RNA to use GlcN6P as a general acid catalyst (Lau and Ferré-D'Amaré 2013). These mutations are therefore consistent with the GlcN6P-independence of *glmS*^{Ca}. Site-directed mutagenesis has previously demonstrated that the phylogenetically conserved guanine at position 40 is essential for the activity of both *glmS*^{WT} and *glmS*^{AAA} (Cochrane et al. 2007; Klein et al. 2007a; Lau and Ferré-D'Amaré 2013). Structural analysis implicated the purine base of this residue in orienting the nucleophile of the transesterification reaction (the 2′-OH of residue −1), and possibly in facilitating its deprotonation (Klein and Ferré-D'Amaré 2006; Cochrane et al. 2007; Klein et al. 2007a). Moreover, Raman crystallographic investigation of the ribozyme demonstrated that G40 contributes to lowering the pK_a of the amine of GlcN6P, the general acid catalytic moiety (Gong et al. 2011). The presence of the G40A mutation in *glmS*^{Ca} thus explains why this ribozyme no longer cleaves its substrates between positions −1 and +1 (Fig. 6). Of the remaining seven mutations, A35U is particularly interesting, as this residue is located in close proximity to the M_A site (Fig. 8), and therefore may be involved in endowing Ca^{2+} selectivity to *glmS*^{Ca}.

Since the ionic radii of Ca^{2+} and Mg^{2+} differ by only 28 pm (Table 2), definitive characterization of the exquisite cation selectivity *glmS*^{Ca} will require atomic-resolution structural analysis of the transition state of the ribozyme. However, none of the mutations that characterize *glmS*^{Ca} disrupt the secondary structure elements that define the unusually stable *glmS* ribozyme fold (Fig. 1B). Therefore, previously determined structures of the RNA can guide provisional interpretation of our results (Fig. 8A,B). Because *glmS*^{Ca} is itself overall structurally stable (indicated by the fact that it can adopt structures indistinguishable by SAXS in the presence of either Mg^{2+}, Ca^{2+}, or Sr^{2+}) (Fig. 5), and because its structure is comparable in compactness to that of the wild-type and *glmS*^{AAA}, the cation selectivity of *glmS*^{Ca} likely results from a localized reorganization of the M_A cation binding site. Our biochemical data are consistent with an enlargement of this site relative to that of the wild-type, such that it cannot achieve tight binding (at least in the transition state) of Mg^{2+} (ionic radius = 86 pm) while being optimal for Ca^{2+} (ionic radius = 114 pm), tolerant for the somewhat larger Sr^{2+} (ionic radius = 132 pm) and unable to accommodate the much larger Ba^{2+} (ionic radius = 149 pm; Table 2). This expansion of the M_A site could be largely the result of the mutation of residue A35, which is immediately adjacent to this cation-binding site, to the smaller uracil (Fig. 8B). The inability of Sr^{2+} to activate a *glmS*^{Ca} ribozyme containing a sulfur substitution of the M_A-coordinating *pro*-R_p NBPO of C2, despite its ability to weakly support catalysis of the unmodified *glmS*^{Ca} (Fig. 4), could hint that replacement of the nonbridging phosphate oxygen with sulfur makes the M_A site too small to accommodate the larger Sr^{2+} cation. In addition, the inability of Cd^{2+} to rescue the same phosphorothioate-containing RNA, despite an ionic radius (109 pm) comparable to

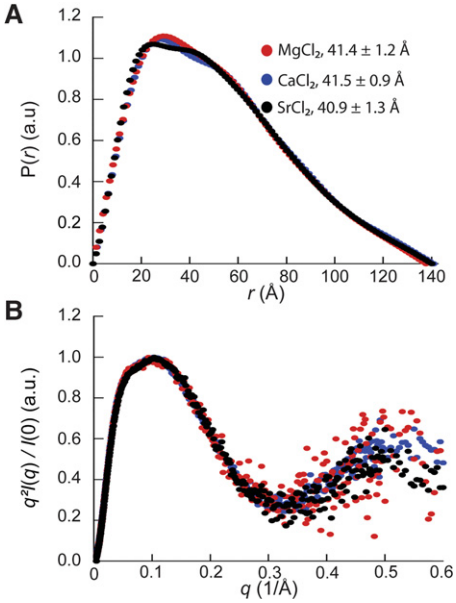

FIGURE 5. SAXS analysis indicates that *glmS*^{Ca} adopts the wild-type fold in a variety of divalent cations. (*A*) Pair-probability functions of *glmS*^{Ca} in the presence of 2.5 mM of either Mg^{2+}, Ca^{2+}, of Sr^{2+} (red, blue, and black, respectively) in addition to 100 mM KCl. The radii of gyration of the RNA in the three divalent cations are indicated (mean ± standard error of the mean of thirty measurements). (*B*) Kratky plots of *glmS*^{Ca} color-coded as in *A*.

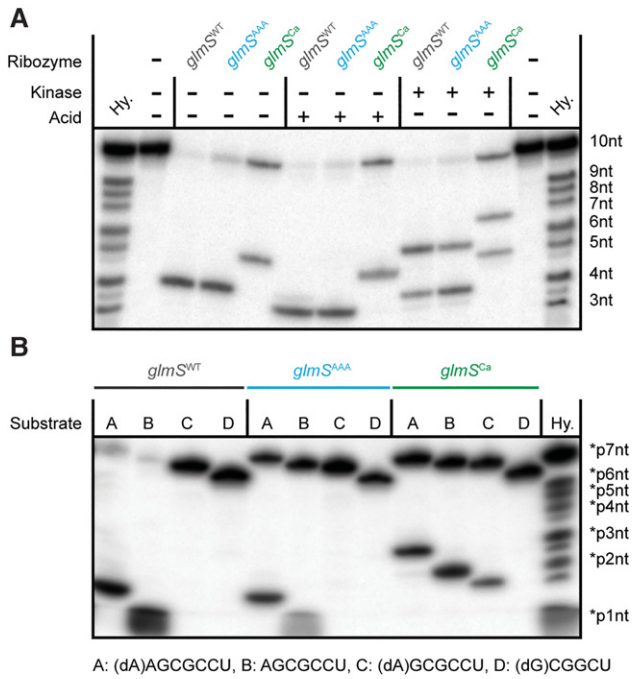

FIGURE 6. Similar to *glmS*^{WT} and *glmS*^{AAA}, *glmS*^{Ca} RNA cleavage proceeds by internal transesterification, but at a site 1 nt distal. (*A*) 5′ Cleavage product end-group analysis. 5′ ^{32}P-radiolabeled substrate was cleaved in *trans* with the three ribozymes for 30 min and treated with acid or with phage T4 polynucleotide kinase prior to analysis by denaturing PAGE, as previously described (Winkler et al. 2004; Xiao et al. 2008; Lau and Ferré-D'Amaré 2013). (*B*) Mapping of *glmS*^{Ca} cleavage site. 5′ ^{32}P-radiolabeled of RNA substrates of varying lengths with or without single-site 2′-deoxy substitutions were cleaved by the three ribozymes and analyzed by denaturing PAGE. (Hy.) Hydrolysis ladder.

that of Ca^{2+} suggests that the remaining ligands of the M_A site, or the substrate atoms with which M_A interacts during catalysis, have a strong preference for hard cations (Table 2).

Compared to the *glmS*^{AAA} ribozyme from which it was selected, *glmS*^{Ca} has adopted a new catalytic strategy that relies on M_A. In the wild-type ribozyme, this cation is structural, since it lies too far away from the cleavage site of that ribozyme (Klein and Ferré-D'Amaré 2006). Moreover, as *glmS*^{WT} is fully active in a variety of metal ions (including cobalt hexammine), its structural cation binding sites (e.g., M_A) have limited selectivity (Roth et al. 2006; Klawuhn et al. 2010). Likewise, *glmS*^{AAA} has only modest cation selectivity, and functions even in high concentrations of the monovalent cation Li^+. Both crystallographic and phosphorothioate interference analyses indicate that M_A retains a structural function in *glmS*^{AAA} (Lau and Ferré-D'Amaré 2013). The co-option of an erstwhile structural metal ion for catalysis (directly or indirectly) by *glmS*^{Ca} is an example of molecular exaptation, that is, the evolutionary repurposing of preexisting features for adaptation to new selective pressures (Gould and Vrba 1982). The evolution of *glmS*^{Ca} illustrates both the rugged fitness landscape of ribozymes, wherein a small number of mutations can have large effects on activity (Pitt and Ferré-D'Amaré 2010; Lau and Ferré-D'Amaré 2016b), and the exceptional structural stability of the triply pseudoknotted *glmS* fold (Hampel and Tinsley 2006; Klein and Ferré-D'Amaré 2006; Tinsley et al. 2007; Lau and Ferré-D'Amaré 2013).

In addition to demonstrating that a self-cleaving ribozyme that requires a metal ion for activity can achieve remarkable specificity for Ca^{2+}, *glmS*^{Ca} is a potentially useful biotechnological tool. Like in the case of the Ca^{2+}-dependent protein nuclease from *Staphylococcus* (Heins et al. 1967), RNA cleavage by *glmS*^{Ca} can be initiated in the presence of Ca^{2+}, and then abruptly stopped by addition of the Ca^{2+}-specific chelator EGTA (Fig. 9). In addition, because this ribozyme is active in modest Ca^{2+} concentrations (~1 mM), it may serve as the basis for new live-cell Ca^{2+} sensors whose output is site-specific RNA cleavage. Organelles such as the endoplasmic reticulum, mitochondria, and nucleus contain total Ca^{2+} levels of ~0.01 to 1 mM. In stimulated tumor mast cells and hyperplastic prostate epithelial cells, this level can reach as high as 1.2 and 7 mM, respectively (Tvedt et al. 1987; Chandra et al. 1994). Such Ca^{2+} concentrations would provide strong and selective activation of *glmS*^{Ca} in vivo.

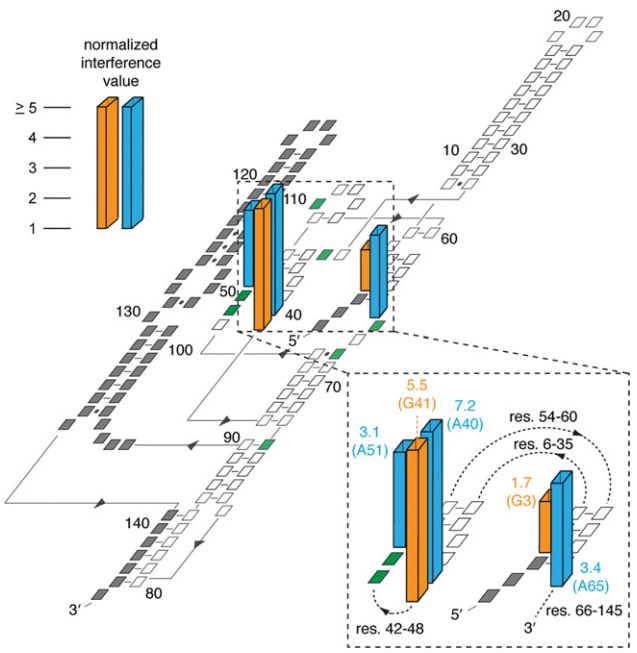

FIGURE 7. Strong phosphorothioate interferences in *glmS*^{Ca}. Normalized interference values (Lau and Ferré-D'Amaré 2013) are shown. Only positions with interferences >1 are shown, and interferences >5 are plotted as having the value 5.0. Interferences from AαS (adenosine phosphorothioate) and GαS are in cyan and orange, respectively. Significant interferences were not observed from CαS and UαS. (*Inset*) Close-up of residues with strong interferences near the active site (res., residue numbers). Residues are colored green and gray in the plane of the secondary structure to represent the eight mutations in *glmS*^{Ca} relative to *glmS*^{AAA}, and positions that were not addressed in the phosphorothioate mapping experiment, respectively.

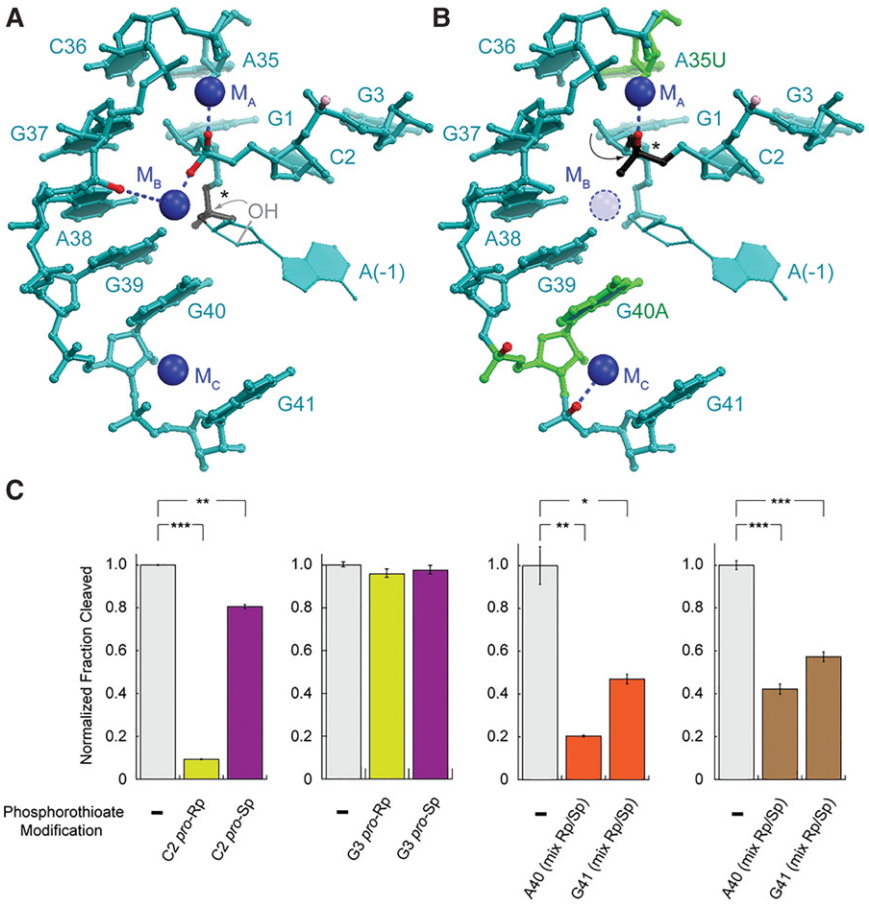

FIGURE 8. *glmS*^{Ca} co-opts a preexisting structural cation for activity. (*A*) The *glmS*^{AAA} active site (Lau and Ferré-D'Amaré 2013). NBPOs with strong and moderate phosphorothioate interference are in red and pink, respectively. Scissile phosphate is in black (*). Residue (−1) is modeled (Lau and Ferré-D'Amaré 2013). (*B*) Phosphorothioate interferences in *glmS*^{Ca} mapped onto the *glmS*^{AAA} structure. Residues that differ between *glmS*^{WT} and *glmS*^{Ca} are in green. (*C*) Effect of NBPO sulfur substitutions on *glmS*^{Ca}. Substitutions of G3 serve as a quality control on the assembly of phosphorothioate-containing ribozymes. Activities of unsubstituted *glmS*^{Ca}, *pro*-Rp, and *pro*-Sp NBPO substitutions, and diastereomeric substitutions are in gray, yellow, purple, and orange, respectively. Sr^{2+} activities are shown in brown. (*), (**), and (***) denote $0.05 < P < 0.01$, $0.001 < P < 0.01$, and $P < 0.001$, respectively (two-tailed *t*-test).

MATERIALS AND METHODS

RNA pool synthesis and selection

A double-stranded mutagenized DNA pool was synthesized as described, with the exception of constant residues A49, A51, and A65 (Fig. 1; Lau and Ferré-D'Amaré 2013, 2016a). Approximately 100 nmol of DNA (~6×10^{15} unique sequences) were used to template transcription of ^{32}P body-labeled RNA for the first selection round. Two parallel selections were performed with 15 nmol of RNA in incubation buffers containing 50 mM HEPES-KOH (pH 7.5), and either 10 mM $MgCl_2$ (Pool A) or 10 mM $CaCl_2$ (Pool B). Active ribozymes were reverse-transcribed as previously described (Lau and Ferré-D'Amaré 2013). In round 2, cDNAs from Pool B were further divided into two before the second PCR step, with one (Pool B) amplified using standard PCR and the other (Pool C) using mutagenic PCR (20 mM Tris–HCl, pH 8.4, 50 mM KCl, 7 mM $MgCl_2$, 0.5 mM $MnCl_2$, 0.2 mM dATPs, 0.2 mM dGTPs, 1 mM dCTPs, 1 mM dTTPs) for 13 cycles (Cadwell and Joyce 1994). Starting with round 3, the divalent cation concentrations in the incubation buffers were reduced to 2 mM, and the 5′ primer was switched to 5′-*TTCTAATACGACTCACTATA*GGTGCACGATCTAAATACTGACCAATCTAAAGGATGCCTAGCGGCTGGACTTAAAGCCGCGAGG-3′ (T7 promoter in italics) during the second PCR step to yield a different leader sequence. A more stringent selection scheme was used starting with round 5, in which RNA pools were 5′ labeled with 6-thioguanosine 5′-monophosphate (^{6S}GMP) and selected using an [(*N*-acryloylamino) phenyl]mercuric chloride (APM) gel mobility-shift assay (Igloi 1988; Lau and Ferré-D'Amaré 2013). A counter-selection step was also introduced starting with round 6 in which ^{6S}GMP tagged RNAs were first incubated overnight in 50 mM HEPES, pH 7.5, with either 25 mM $CaCl_2$, 25 mM $MgCl_2$, or 25 mM $MnCl_2$ for Pools A, B, and C, respectively. RNAs that did not self-cleave were recovered by electrophoresis through APM gels, and ribozymes specifically active in either Mg^{2+} or Ca^{2+} were selected using conditions described above.

Kinetics

Ribozyme rate measurements in different metal ion conditions were performed as previously described (Lau and Ferré-D'Amaré 2013). For determination of the inhibitory effects of Mg^{2+} and Ba^{2+} on *glmS*^{Ca} activity, 5 mM $MgCl_2$ or 5 mM $BaCl_2$ was added to cleavage reactions in varying concentrations of $CaCl_2$ (from 2 to 150 mM). Pseudo–first-order rates were determined as previously described (Lau and Ferré-D'Amaré 2013). All cleavage rate measurements were performed on a background of 100 mM KCl.

Small-angle X-ray scattering

SAXS experiments were performed at beamline 12-ID-C of The Advanced Photon Source at Argonne National Laboratories. Unimolecular *glmS* ribozyme constructs were used in this study, rather than the bimolecular RNAs used by Lau and Ferré-D'Amaré (2013). The constructs correspond to those in Figure 1A, except that their first nucleotide is residue +1. RNA samples were extensively exchanged into a solution containing 20 mM HEPES-KOH pH 7.5, 100 mM KCl, and 10 μM EDTA using Millipore Amicon Ultra centrifugal concentrators (10 kDa molecular weight cutoff). The samples were then prepared for analysis on-site by heating to 85°C for 2 min, followed by buffer exchange into the buffer listed above, supplemented with 2.5 mM of the

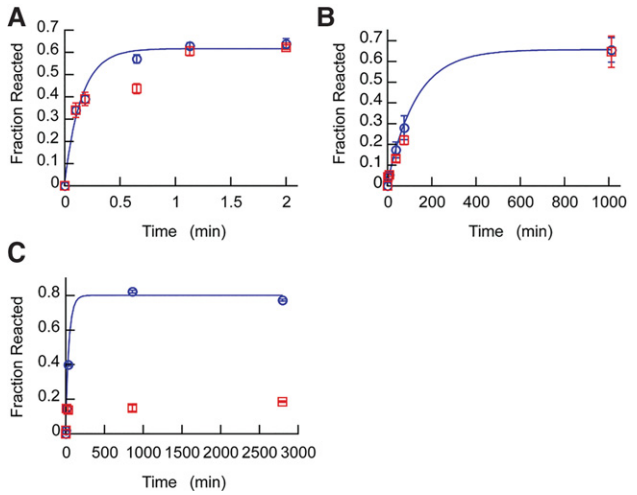

FIGURE 9. Chelation of Ca^{2+} by EGTA halts $glmS^{Ca}$, but not $glmS^{WT}$ or $glmS^{AAA}$ under physiological cation concentrations. Reaction time courses for (*A*) $glmS^{WT}$ (in the presence of 25 µM GlcN6P), (*B*) $glmS^{AAA}$, and (*C*) $glmS^{Ca}$ were initiated by the addition of both 25 mM Mg^{2+} and 25 mM Ca^{2+}. After the second time point, half of the sample from each reaction was transferred into a fresh tube containing a twofold molar excess of EGTA. The reactions with (red) or without EGTA (blue) added were continued for the remaining time points. First-order rate fits are shown for reactions with no EGTA added (blue). Error bars are standard errors of the mean from three independent time courses.

appropriate group II divalent ion. Samples were then passed through a Durapore PVDF 0.1 µm filter prior to UV/Vis analysis and SAXS data collection. Samples were allowed to equilibrate at room temperature for 30 min prior to collection. Samples, ranging from 0.7–1.5 mg/mL, were passed through a flow cell, during which they were exposed to the X-ray beam (12 keV) for 0.5 sec, followed by a 2.0 s rest time. Thirty data sets were collected per sample using a Pilatus 2M detector. Prior to averaging, each data set was examined for radiation damage and aggregation using Igor Pro (WaveMetrics). Guinier analysis was performed using Igor Pro. Indirect Fourier transformation was performed using the programs DATGNOM and GNOM (Svergun 1992; Petoukhov et al. 2007).

Phosphorothioate interference mapping and NBPO substitution experiments

Phosphorothioate interference mapping was performed using 185-nt *cis*-cleaving $glmS^{Ca}$ constructs, and interference values were calculated as previously described (Lau and Ferré-D'Amaré 2013). For individual NBPO substitution experiments, RNA oligos 5′-AG*CGCCU-3′ and 5′-AGC*GCCU-3′ ([*] indicates position of diastereomeric phosphorothioate substitutions) were purchased from Dharmacon. Rp and Sp phosphorothioate isomers were resolved by reversed-phase HPLC (Frederiksen and Piccirilli 2009). Rates for NBPO substitutions at C2 or G3 were determined by incubation of HPLC-purified RNA oligos (Rp or Sp), respectively, with a 126-nt *trans*-acting $glmS^{Ca}$ construct in 25 mM HEPES-KOH, pH 7.5, 5 mM $CaCl_2$. Of note, 126-nt *trans*-acting $glmS^{Ca}$ constructs containing diastereomeric sulfur substitutions at the NBPOs of A40 or G41 were synthesized by enzymatic ligation of a 104 nt $glmS^{Ca}$ ribozyme truncated to start at position 42 (CAGGGU… CAGGAA), with RNA oligo 5′-GGCUUUAAGUUGUCGAG* AG-3′ and 5′-GGCUUUAAGUUGUCGAGA*G-3′, respectively. The ligated RNAs were purified by 8% denaturing PAGE. The ribozymes were incubated with 5′ ^{32}P-labeled RNA oligo 5′-AGCGCCU GGACUUAAAGCC-3′ to determine the effects of A40 or G41 NBPO substitutions. The same RNA constructs and conditions were used for Sr^{2+} experiments, except 5 mM Ca^{2+} was replaced with 5 mM Sr^{2+}.

ACKNOWLEDGMENTS

We thank J. Sellers for access to rapid-quench instrumentation, X. Zuo and the staff at beamline 12-ID-C of the Advanced Photon Source (APS), Argonne National Laboratory (ANL) for SAXS data collection support, S. Bachas, N. Baird, M. Chen, T. Dever, J. Hogg, C. Jones, J. Posakony, K. Warner, and J. Zhang for discussions, and two anonymous referees for motivating the SAXS experiments and suggesting the inclusion of Table 2. M.W.L. was a Croucher Foundation Postdoctoral Fellow. SAXS data were collected in a core facility of the Center for Cancer Research, US National Cancer Institute (NCI), allocated under an agreement between NCI and ANL (PUP-24152). Use of APS was supported by the US Department of Energy. This work was supported in part by the Intramural Program of the National Heart, Lung and Blood Institute, National Institutes of Health (NIH).

Received October 28, 2016; accepted November 28, 2016.

REFERENCES

Aufinger P, Grover N, Westhof E. 2011. Metal ion binding to RNA. *Met Ions Life Sci* **9:** 1–35.

Cadwell RC, Joyce GF. 1994. Mutagenic PCR. *PCR Methods Appl* **3:** S136–S140.

Celander DW, Cech TR. 1991. Visualizing the higher order folding of a catalytic RNA molecule. *Science* **251:** 401–407.

Cernak P, Madix RA, Kuo LY, Lehman N. 2008. Accommodation of Ca (II) ions for catalytic activity by a group I ribozyme. *J Inorg Biochem* **102:** 1495–1506.

Chandra S, Fewtrell C, Millard PJ, Sandison DR, Webb WW, Morrison GH. 1994. Imaging of total intracellular calcium and calcium influx and efflux in individual resting and stimulated tumor mast cells using ion microscopy. *J Biol Chem* **269:** 15186–15194.

Clapham DE. 2007. Calcium signaling. *Cell* **131:** 1047–1058.

Cochrane JC, Lipchock SV, Strobel SA. 2007. Structural investigation of the GlmS ribozyme bound to its catalytic cofactor. *Chem Biol* **14:** 97–105.

Cochrane JC, Lipchock SV, Smith KD, Strobel SA. 2009. Structural and chemical basis for glucosamine 6-phosphate binding and activation of the *glmS* ribozyme. *Biochemistry* **48:** 3239–3246.

Collins JA, Irnov I, Baker S, Winkler WC. 2007. Mechanism of mRNA destabilization by the *glmS* ribozyme. *Genes Dev* **21:** 3356–3368.

Cowan JA. 1993. Metallobiochemistry of RNA. $Co(NH_3)_6^{3+}$ as a probe for Mg^{2+} (aq) binding sites. *J Inorg Biochem* **49:** 171–175.

Draper DE. 2004. A guide to ions and RNA structure. *RNA* **10:** 335–343.

Fedor MJ, Williamson JR. 2005. The catalytic diversity of RNAs. *Nat Rev Mol Cell Biol* **6:** 399–412.

Fei X, Holmes T, Diddle J, Hintz L, Delaney D, Stock A, Renner D, McDevitt M, Berkowitz DB, Soukup JK. 2014. Phosphatase-inert glucosamine 6-phosphate mimics serve as actuators of the glmS riboswitch. *ACS Chem Biol* **9:** 2875–2882.

Ferré-D'Amaré AR. 2010. The *glmS* ribozyme: use of a small molecule coenzyme by a gene-regulatory RNA. *Q Rev Biophys* **43:** 423–447.

Ferré-D'Amaré AR. 2011. Use of a coenzyme by the *glmS* ribozyme-riboswitch suggests primordial expansion of RNA chemistry by small molecules. *Philos Trans R Soc Lond B Biol Sci* **366:** 2942–2948.

Ferré-D'Amaré AR, Scott WG. 2010. Small self-cleaving ribozymes. *Cold Spring Harbor Persp Biol* **2:** a003574.

Frank DN, Pace NR. 1997. *In vitro* selection for altered divalent metal specificity in the RNase P RNA. *Proc Nat Acad Sci* **94:** 14355–14360.

Frederiksen JK, Piccirilli JA. 2009. Separation of RNA phosphorothioate oligonucleotides by HPLC. *Methods Enzymol* **468:** 289–309.

Gong B, Klein DJ, Ferré-D'Amaré AR, Carey PR. 2011. The *glmS* ribozyme tunes the catalytically critical pK_a of its coenzyme glucosamine-6-phosphate. *J Am Chem Soc* **133:** 14188–14191.

Gould SJ, Vrba ES. 1982. Exaptation—a missing term in the science of form. *Paleobiology* **8:** 4–15.

Grosshans CA, Cech TR. 1989. Metal ion requirements for sequence-specific endoribonuclease activity of the *Tetrahymena* ribozyme. *Biochemistry* **28:** 6888–6894.

Grubbs RD. 2002. Intracellular magnesium and magnesium buffering. *Biometals* **15:** 251–259.

Hampel KJ, Tinsley MM. 2006. Evidence for preorganization of the *glmS* ribozyme ligand binding pocket. *Biochemistry* **45:** 7861–7871.

Heins JN, Suriano JR, Taniuchi H, Anfinsen CB. 1967. Characterization of a nuclease produced by *Staphylococcus aureus*. *J Biol Chem* **242:** 1016–1020.

Huheey JE. 1983. *Inorganic chemistry principles of structure and reactivity*. Harper International, Cambridge, MA.

Igloi GL. 1988. Interaction of tRNAs and of phosphorothioate-substituted nucleic acids with an organomercurial. Probing the chemical environment of thiolated residues by affinity electrophoresis. *Biochemistry* **27:** 3842–3849.

Klawuhn K, Jansen JA, Souchek J, Soukup GA, Soukup JK. 2010. Analysis of metal ion dependence in *glmS* ribozyme self-cleavage and coenzyme binding. *Chembiochem* **11:** 2567–2571.

Klein DJ, Ferré-D'Amaré AR. 2006. Structural basis of *glmS* ribozyme activation by glucosamine-6-phosphate. *Science* **313:** 1752–1756.

Klein DJ, Been MD, Ferré-D'Amaré AR. 2007a. Essential role of an active-site guanine in *glmS* ribozyme catalysis. *J Am Chem Soc* **129:** 14858–14859.

Klein DJ, Wilkinson SR, Been MD, Ferré-D'Amaré AR. 2007b. Requirement of helix P2.2 and nucleotide G1 for positioning of the cleavage site and cofactor of the *glmS* ribozyme. *J Mol Biol* **373:** 178–189.

Koculi E, Hyeon C, Thirumalai D, Woodson SA. 2007. Charge density of divalent metal cations determines RNA stability. *J Am Chem Soc* **129:** 2676–2682.

Lau MWL, Ferré-D'Amaré AR. 2013. An *in vitro* evolved *glmS* ribozyme has the wild-type fold but loses coenzyme dependence. *Nat Chem Biol* **9:** 805–810.

Lau MWL, Ferré-D'Amaré AR. 2016a. *In vitro* evolution of coenzyme-independent variants from the *glmS* ribozyme structural scaffold. *Methods* **106:** 76–81.

Lau MWL, Ferré-D'Amaré AR. 2016b. Many activities, one structure: functional plasticity of ribozyme folds. *Molecules* **21:** E1570.

Lehman N, Joyce GF. 1993. Evolution *in vitro* of an RNA enzyme with altered metal dependence. *Nature* **361:** 182–185.

Lim J, Grove BC, Roth A, Breaker RR. 2006. Characteristics of ligand recognition by a *glmS* self-cleaving ribozyme. *Angew Chem Int Ed Engl* **45:** 6689–6693.

McCarthy TJ, Plog MA, Floy SA, Jansen JA, Soukup JK, Soukup GA. 2005. Ligand requirements for *glmS* ribozyme self-cleavage. *Chem Biol* **12:** 1221–1226.

Parr RG, Pearson RG. 1983. Absolute hardness: companion parameter to absolute electronegativity. *J Am Chem Soc* **105:** 7512–7516.

Pearson RG. 1988. Absolute electronegativity and hardness: application to inorganic chemistry. *Inorg Chem* **27:** 734–740.

Petoukhov MV, Konarev PV, Kikhney AG, Svergun DI. 2007. ATSAS 2.1—towards automated and web-supported small-angle scattering data analysis. *J Appl Crystallogr* **40:** s223–s228.

Pitt JN, Ferré-D'Amaré AR. 2010. Rapid construction of empirical RNA fitness landscapes. *Science* **330:** 376–379.

Posakony JJ, Ferré-D'Amaré AR. 2013. Glucosamine and glucosamine-6-phosphate derivatives: catalytic cofactor analogues for the *glmS* ribozyme. *J Org Chem* **78:** 4730–4743.

Riley CA, Lehman N. 2003. Expanded divalent metal-ion tolerance of evolved ligase ribozymes. *Biochimie* **85:** 683–689.

Romani A, Scarpa A. 1992. Regulation of cell magnesium. *Arch Biochem Biophys* **298:** 1–12.

Roth A, Nahvi A, Lee M, Jona I, Breaker RR. 2006. Characteristics of the *glmS* ribozyme suggest only structural roles for divalent metal ions. *RNA* **12:** 607–619.

Schatz D, Leberman R, Eckstein F. 1991. Interaction of *Escherichia coli* $tRNA^{Ser}$ with its cognate aminoacyl-tRNA synthetase as determined by footprinting with phosphorothioate-containing tRNA transcripts. *Proc Natl Acad Sci* **88:** 6132–6136.

Svergun DI. 1992. Determination of the regularization parameter in indirect-transform methods using perceptual criteria. *J Appl Crystallogr* **25:** 495–503.

Tinsley RA, Furchak JR, Walter NG. 2007. *Trans*-acting *glmS* catalytic riboswitch: locked and loaded. *RNA* **13:** 468–477.

Tvedt KE, Kopstad G, Haugen OA, Halgunset J. 1987. Subcellular concentrations of calcium, zinc, and magnesium in benign nodular hyperplasia of the human prostate: X-ray microanalysis of freeze-dried cryosections. *Cancer Res* **47:** 323–328.

Viladoms J, Fedor MJ. 2012. The *glmS* ribozyme cofactor is a general acid-base catalyst. *J Am Chem Soc* **134:** 19043–19049.

Winkler WC, Nahvi A, Roth A, Collins JA, Breaker RR. 2004. Control of gene expression by a natural metabolite-responsive ribozyme. *Nature* **428:** 281–286.

Xiao H, Murakami H, Suga H, Ferré-D'Amaré AR. 2008. Structural basis of specific tRNA aminoacylation by a small *in vitro* selected ribozyme. *Nature* **454:** 358–361.